Supporting Information

Boosting the AIEgen-based Photo-theranostic Platform by Balancing Radiative Decay and Non-Radiative Decay

Yanzi Xu,[a] Dongfeng Dang,[a] Hongrui Zhu,[b] Xunan Jing,[a] Xun Zhu,[c] Ning Zhang,[a] Chunbin Li,[d] Yizhen Zhao,[c] Pengfei Zhang,[d] Zhiwei Yang,*[c] Lingjie Meng*[a,e]*

[a] School of Chemistry, Xi'an Key Laboratory of Sustainable Energy Material Chemistry, Xi'an Jiao Tong University, Xi'an 710049, P. R. China.

[b] Key Laboratory of Biomedical Information Engineering of Education Ministry, School of Life Science and Technology, Xi'an Jiao Tong University, Xi'an 710049, P. R. China.

[c] School of Physics, MOE Key Laboratory for Nonequilibrium Synthesis and Modulation of Condensed Matter, Xi'an Jiaotong University, Xi'an 710049, China.

[d] Guangdong Key Laboratory of Nanomedicine, CAS Key Laboratory of Health Informatics, Shenzhen Bioactive Materials Engineering Lab for Medicine, Institute of Biomedicine and Biotechnology, Shenzhen Institutes of Advanced Technology, Chinese Academy of Sciences, Shenzhen, 518055 P. R. China.

[e] Instrumental analysis center, Xi'an Jiao Tong University Xi'an 710049, P. R. China.

E-mail: dongfengdang@xjtu.edu.cn

yzws-123@mail.xjtu.edu.cn, menglingjie@xjtu.edu.cn

Experimental section

Synthesis

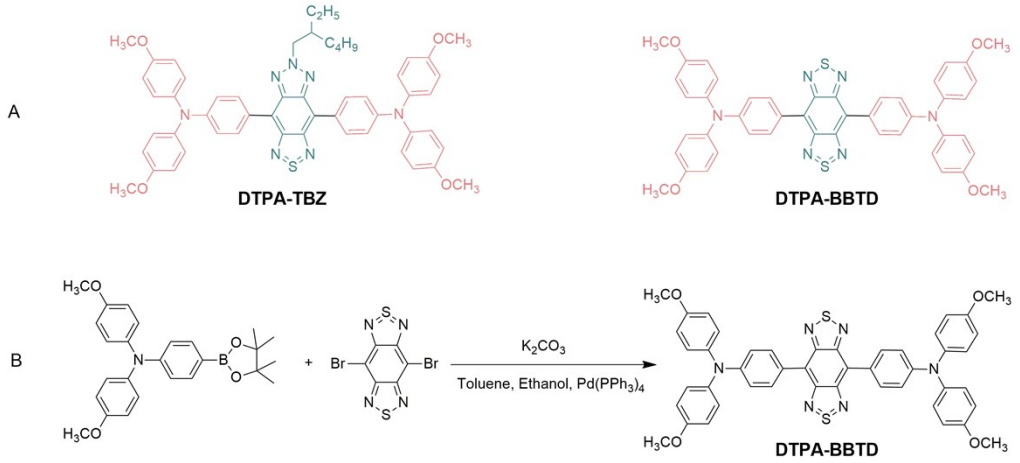

Figure S1. Chemical structures of DTPA-TBZ and DTPA-BBTD (A); Synthetic route to DTPA-BBTD (B).

Synthesis of DTPA-BBTD

To the toluene (80 mL) solution of N,N-bis(4-methoxyphenyl)-4- (4,4,5,5-tetramethyl-1,3,2-dioxaborolan-2-yl)-benzenamine (294.07 mg, 0.68 mmol) and benzo[1,2-c:4,5-c']bis([1,2,5]thiadiazole (BBTD, 100 mg, 0.28 mmol), ethanol and potassium carbonate (K_2CO_3) (2 M, 3.55 mL), tetrakis(triphenylphosphine)palladium [$Pd(PPh_3)_4$, 16.4 mg] was added under nitrogen. After stirring at 85 ^oC for 17 h, the mixture was quenched with water (10 mL) and then was extracted with dichloromethane (DCM) three times (3×30 mL). After that, the obtained organic solution was dried over anhydrous magnesium sulfate ($MgSO_4$). By following the filtration and then removing the solvent, the crude product was finally obtained. After purification with recrystallization by using chloroform as a solvent, the deep green powder of DTPA-BBTD was finally obtained with a yield of 17%. ^1H NMR (400 MHz, $CDCl_3$) δ = 8.13 (d, *J* = 8.0 Hz, 4H), 7.20 (d, *J* = 8.0 Hz, 8H), 7.12 (d, *J* = 12.0 Hz, 4H), 6.89 (d, *J* = 12.0 Hz, 8H), 3.82 (s, 12H). ^{13}C NMR (100 MHz, $CDCl_3$) δ = 156.43, 152.78, 149.18, 140.17, 132.57, 127.51, 126.70, 120.00, 118.66, 114.81, 55.50 ppm; HRMS (TOF-ESI+): *m/z* calculated for [Mt] $C_{46}H_{36}N_6O_2S_4^+$ ($[M+H]^+$), 801.2273; Found, 801.2291.

Synthesis of DTPA-TBZ

The synthetic route of DTPA-TBZ is similar to DTPA-BBTD by using N,N-bis(4-methoxyphenyl)-4-(4,4,5,5-tetramethyl-1,3,2-dioxaborolan-2-yl)-benzenamine and 4,8-dibromo-6-(2-ethylhexyl)-[1,2,5]thiadiazolo[3,4-f]benzotriazole as reactant.[1] And DTPA-TBZ as a deep blue powder with a yield of 78% was finally obtained. ^{1}H NMR (400 MHz, $CDCl_3$) δ = 8.31 (d, *J* = 8.0 Hz, 4H), 7.19 (d, *J* = 8.0 Hz, 8H), 7.11 (d, *J* = 8.0 Hz, 4H), 6.88 (d, *J* = 8.0 Hz, 8H), 4.77 (d, *J* = 84.0 Hz, 2H), 3.82 (s, 12H), 1.38 (m, 6H), 1.28 (m, 3H), 0.95 (t, *J* = 8.0 Hz, 3H), 0.85 (t, *J* = 8.0 Hz, 3H). ^{13}C NMR (100 MHz, $CDCl_3$) δ = 156.22, 151.50, 148.65, 144.36, 140.07, 131.96, 127.28, 126.76, 119.17, 114.73, 61.17, 55.50, 30.59, 29.69, 28.39, 24.01, 22.96, 14.03, 10.52 ppm; HRMS (TOF-ESI+): *m/z* calculated for [Mt] $C_{54}H_{53}N_7O_4S^+$ ($[M+H]^+$), 896.3913; Found, 896.3910.

Fabrication of DTPA-BBTD-based AIE dots

A mixture of DTPA-BBTD (1.0 mg), FA-DSPE-PEG2000 (2 mg) and THF (1 mL) was added in a centrifuge tube and sonicated for 15 min to acquire a clear solution. Then the solution (100 μL) was immediately injected into 5 mL of vigorously stirring ultra-pure water for 5 min. The dispersion was then stirred for 15 minutes at room temperature to remove the residual THF. Finally, the AIE dots were filtered by a membrane filter with a diameter of 0.22 μm and subsequently subjected to 1.0 mg/mL by using an ultrafiltration (Corning, M_w = 30 K). The AIE dots were stored in refrigerator at 4 °C for further using.

Fluorescence QY measurement of DTPA-BBTD-based AIE dots

The fluorescence quantum yield (QY) of DTPA-BBTD-based AIE dots was measured by utilizing NIR-II fluorescent IR-26 dye as the reference (QY = 0.5%). A stock solution of IR-26 in 1, 2-dichloroethane (DCE) was initially prepared and then diluted to obtain a series of solutions with absorbance values of ~ 0.10, ~ 0.08, ~ 0.06, ~ 0.04, and ~ 0.02 at 808 nm. The emission spectra was recorded by using a 808 nm pulse laser as the excitation source and a 850 nm long-pass filter in the 900-1500 nm region to reject the excitation light. Same procedures were executed for the DTPA-

BBTD-based AIE dots in an aqueous solution. The acquired integrated NIR-II fluorescence intensity was plotted against absorbance value at 808 nm and fitted into a linear function. The obtained two slopes were utilized for calculating the QY based on this method: one was collected for the IR-26 in DCE as reference and the other was recorded for AIE dots sample. The quantum yield of the DTPA-BBTD-based AIE dots in aqueous solution can be acquired by the following equation:

$$QY_{sample} = QY_{ref} \times \frac{Slope_{sample}}{Slope_{ref}} \times \left(\frac{\eta_{sample}}{\eta_{ref}} \right)^2$$

Here, QY_{ref} is defined as 0.5%. η_{sample} and η_{ref} are the refractive index of water and DCE, respectively.

Density Functional Theory (DFT) calculation and Molecular dynamics (MD) simulations

In according with our previous works[1], the optimizations of geometry configuration and energy distribution of each compound in single molecule (DTPA-TBZ and DTPA-BBTD) were performed by using the density functional theory (DFT) method at the B3LYP/6-31G (d,p) level. The original configuration of each aggregate (DTPA-TBZ-A and DTPA-BBTD-A) was obtained by random placing 40 optimized molecules in a 8.0×8.0×8.0 nm cubic simulation box[2]. Each system was then refined by the 25.0 ns molecular dynamics (MD) simulations with the Amber 18 and GAFF2 force field. The details of the MD simulation setup are consistent with previous works[3]. Briefly, each system was dissolved with TIP3P waters in an isothermal, isobaric ensemble (NPT, T= 298 K and P= 1 atm) with periodic boundary conditions. Free dynamics were performed using a 1.0 fs time step, and coordinates were collected every 5.0 ps. The Cpptraj module of AmberTools was utilized for analyzing the trajectories. The dihedral angles, the radius of gyration (RoG), the root-mean-square fluctuation (RMSF), and density of each system were collected to assess the cross-validation of structural dynamics.

In Vitro Cytotoxicity Assay

The cytotoxicity of DTPA-BBTD-based AIE dots were measured by WST-1

assay. Initially, 4T1 cells were carefully seeded onto fresh 96-well plates with a density of 5×10^6 cells per well in 100 μL and cultured for 12 h. The DTPA-BBTD-based AIE dots were then injected into the wells with different concentrations (0, 10, 20, 30, 40, and 50 μg/mL, respectively) and then were further co-cultivated for 24 h. After that, the detective reagents WST-1 assay was employed to evaluate the viability of cells. During the procedure, the absorbance at 450 nm was first recorded by a microplate reader, then the AIE dots were removed and a fresh aliquot of DMEM (100 μL) containing WST-1 solution (10 μL) was injected into each well. The cells were incubated at 37 °C in 5% of CO_2 for another 4 h. Their absorbance at 450 nm (reference wavelength) was also collected. The relative viability of the 4T1 cells was calculated by comparing the absorbance in DTPA-BBTD dots-treated cells and the absorbance in the control group (The untreated cells defined as the control groups and their viability was set as 100%). For PTT treatment, the plate was irradiated with a 660 nm laser (1 W cm^{-2}, 5 min) after 6 h incubation with various formulations and further incubated for another 24 h. Next, the standard WST-1 assay was employed to calculate the inhibition effect of DTPA-BBTD dots. All the experiments were carried out in quintuplicate.

Animal Experiment

The animal experiments were carried out strictly in accordance with the requirements and guidelines of the Animal Management Rules of Ministry of Health of the People's Republic of China. Female BALB/c nude mice (weight = 16-18 g) were obtained from the Beijing Vital River Laboratory Animal Technology Co. Ltd. (Beijing, China). The animal treatments were in compliance with the protocols evaluated and approved by the Ethical Committee of the Xi'an Jiao Tong University. The tumor model of breast cancer was established by injecting 4T1 tumor cells ($\approx 1 \times 10^6$) subcutaneously into the upper right leg of the mice and waiting for its growth for about a week to make the tumor diameter reach 6-8 mm.

In Vivo fluorescence and PA Imaging

For the fluorescence imaging *in vivo* in NIR-II window, the mice were

intravenously injected with DTPA-BBTD-based AIE dots (1 mg/mL, 120 μL) and the images were collected *via* a NIR-OPTICS Series III 900/1700 small animal imaging system (Suzhou NIR-Optics Technology Co., Ltd.) equipped with a 1000 nm long pass filter. The diode laser (808 nm, 1 W/cm^2) was utilized as the excitation source in the NIR-II fluorescence imaging system with an exposure time of 150 ms. The PA microscopy system (FujiFilm VisualSonics) was used to record the images over different time points, where a pulsed laser (860 nm) was used in the PA imaging system.

In Vivo Photothermal therapy

BALB/c mice bearing4T1-tumors were randomly divided into 3 groups (n = 3/group) with various treatment conditions by intravenously injection: PBS injection as the control group, DTPA-BBTD dots without laser and DTPA-BBTD dots with laser. Therapy was sustained for 14 days through tail vein injection. Mice were injected (at day 0, day 4, day 8) with the corresponding AIE dots at the dose of 1 mg mL^{-1}, 120 μL. For PTT treatment, the mice were locally irradiated with a 660 nm laser (1 W cm^{-2}, 10 min) after 24 h injection. The body weight and the tumor size of each mouse were collected to assess the curative effect and side effects. Finally, the experimental mice were sacrificed and blood samples were gathered into tubes containing 1.5 mg/mL K_2EDTA for blood cell count after 14th treatment. Plasma was separated into cryotubes and store at -80 ^{o}C until blood chemistry analysis. Major organs (heart, liver, spleen, lung, kidney and tumor) were sliced up for H&E staining.

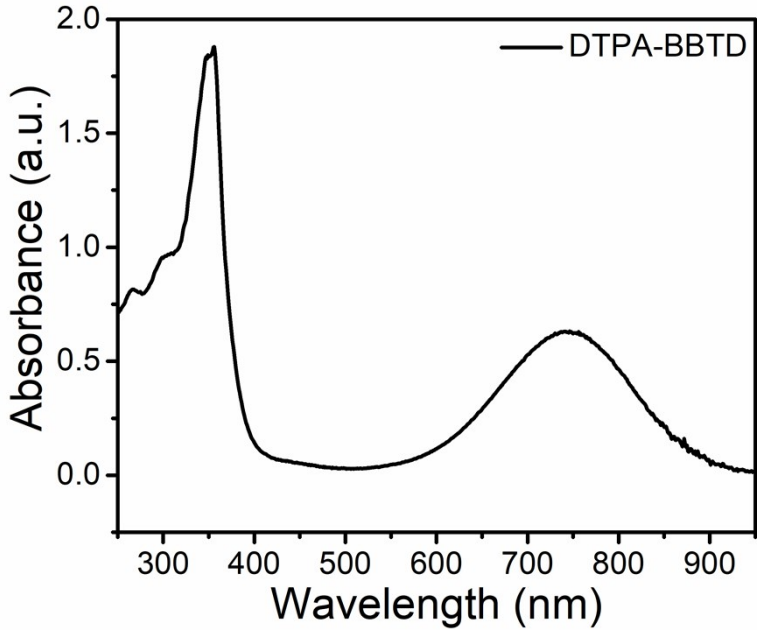

Figure S2. UV-vis absorption spectrum of DTPA-BBTD in THF solution ([*c*]= 1×10^{-5} mol/L).

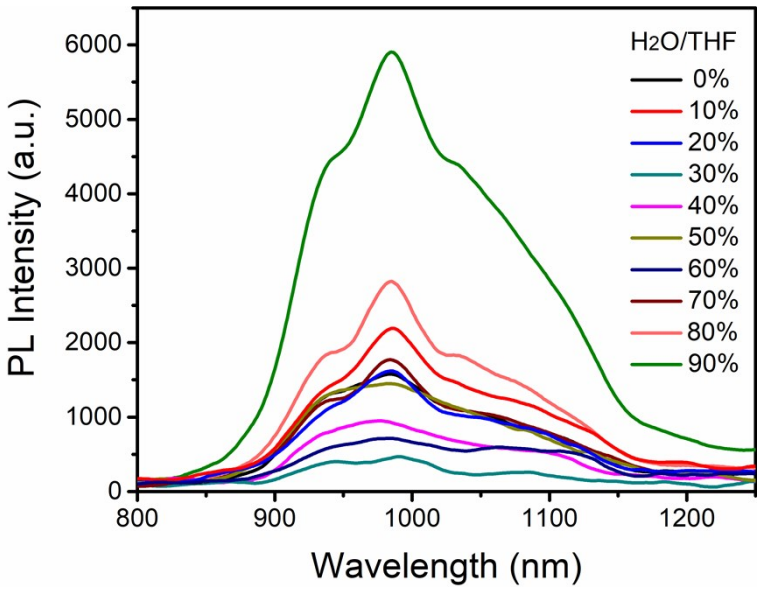

Figure S3. PL spectra of DTPA-BBTD in a THF/water mixture with various water fractions (f_w).

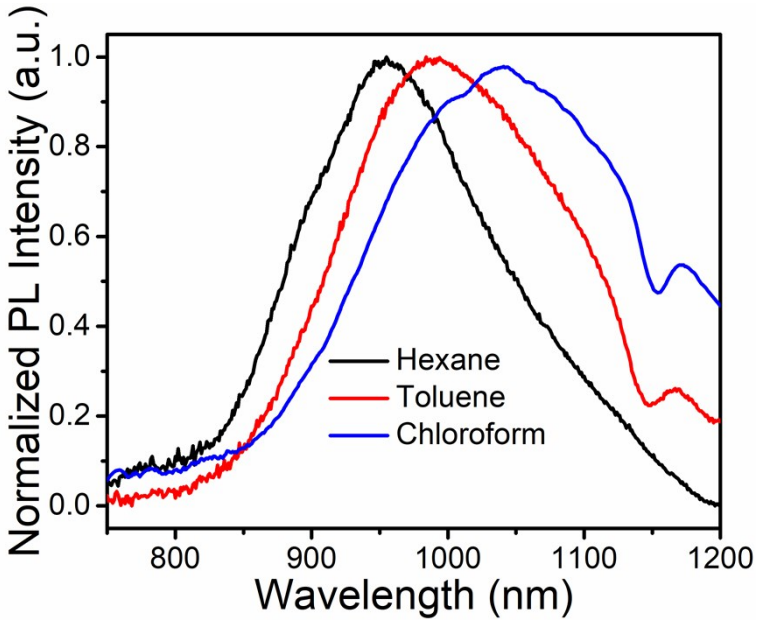

Figure S4. Normalized PL spectra of DTPA-BBTD in various solvents with different polarities.

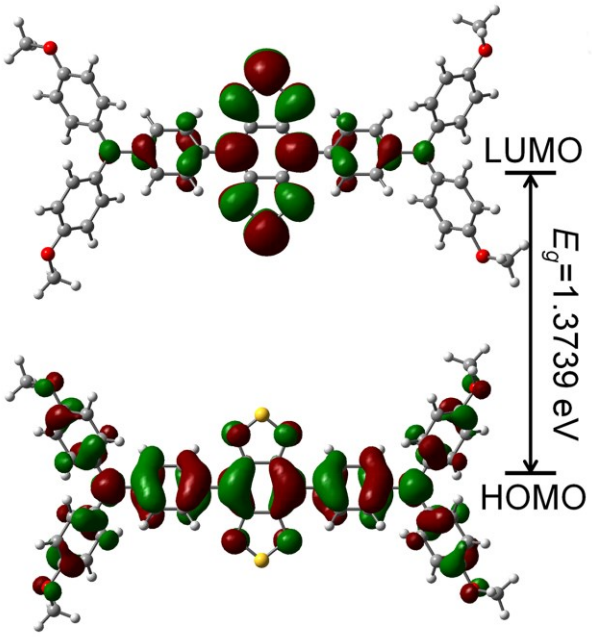

Figure S5. Electron density distribution of molecular orbitals (HOMO and LUMO) in DTPA-BBTD.

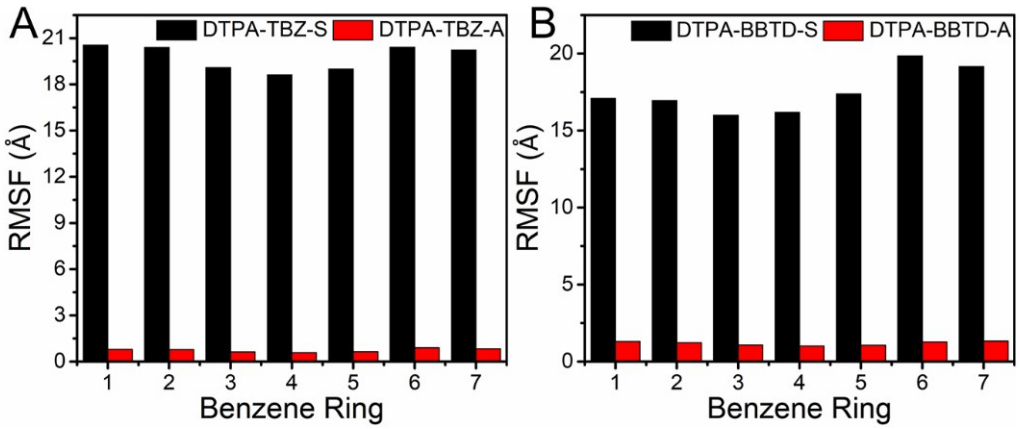

Figure S6. Root-mean-square fluctuation (RMSF) values of each phenyl ring over MD simulations for DTPA-TBZ (A) and DTPA-BBTD (B) in single molecule and aggregates (single molecule is abbreviated as S, molecule in aggregates is abbreviated as A).

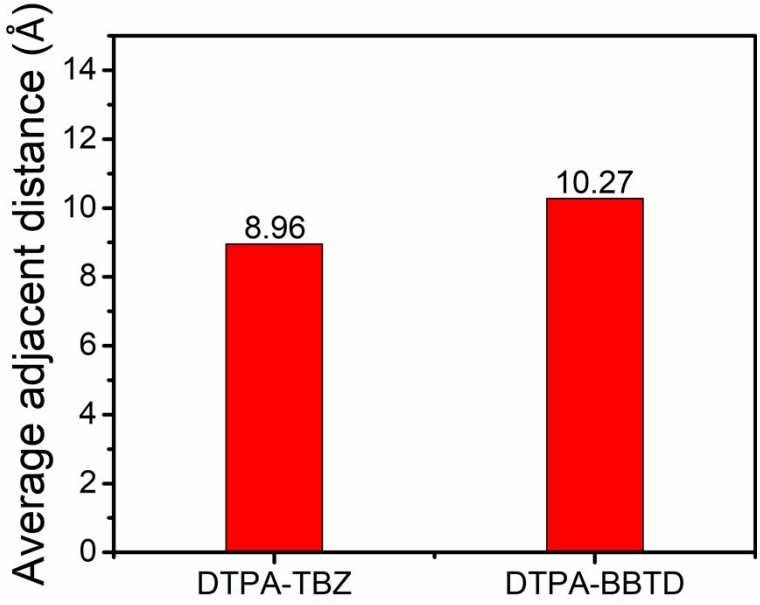

Figure S7. The average distance between adjacent molecule in DTPA-TBZ and DTPA-BBTD, respectively.

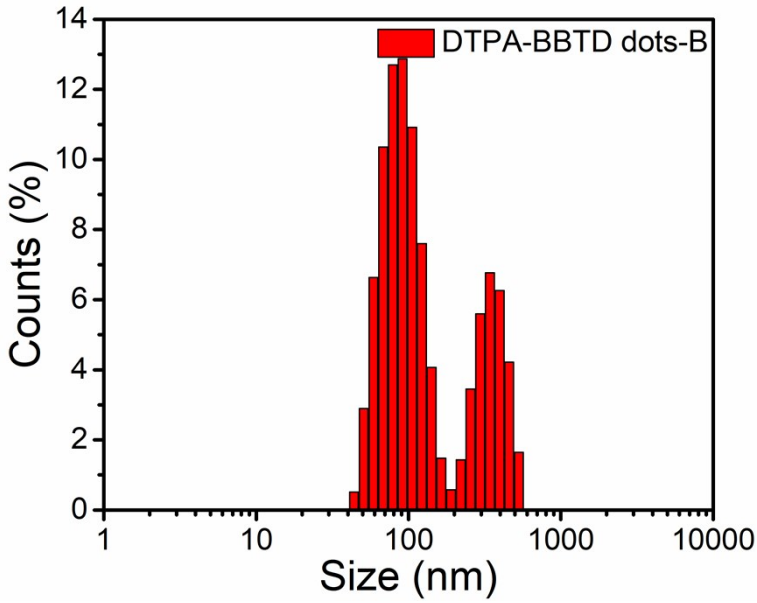

Figure S8. DLS distribution of DTPA-BBTD dots without the capsulation of FA-DSPE-PEG2000.

.

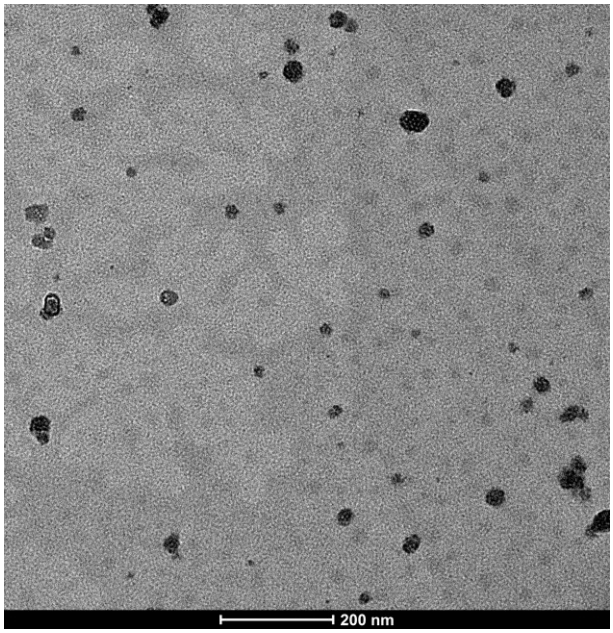

Figure S9. TEM image of DTPA-BBTD dots without the capsulation of FA-DSPE-PEG2000.

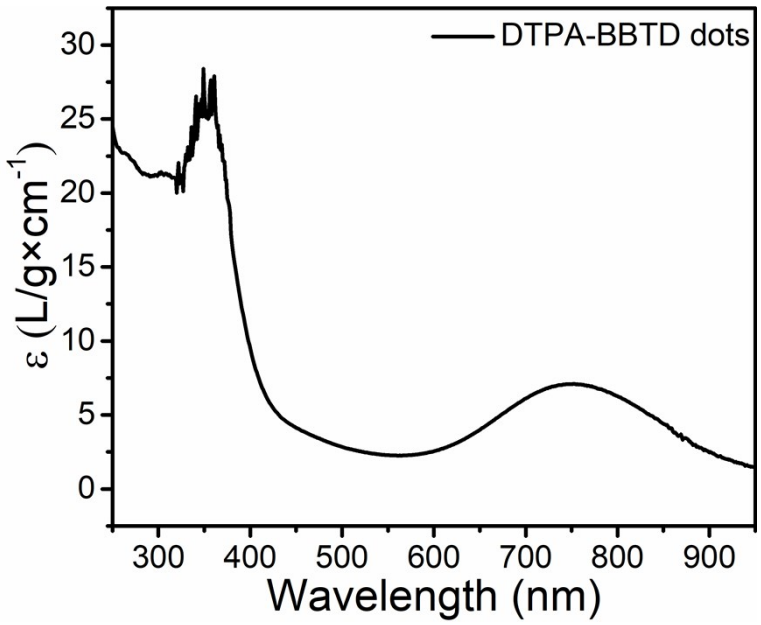

Figure S10. Molar extinction coefficient of DTPA-BBTD-based AIE dots in aqueous dispersion ([*c*]= 100 μg/mL).

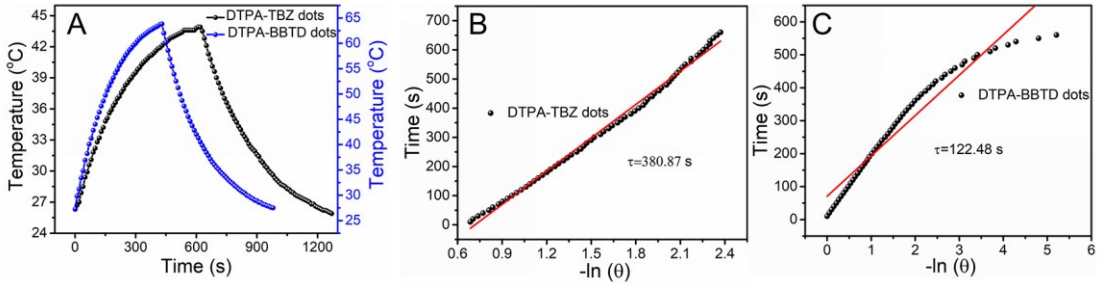

Figure S11. (A) Photothermal heating and cooling curves of DTPA-TBZ-based AIE dots and DTPA-BBTD-based AIE dots ([*c*]= 200 μg/mL) upon laser irradiation (660 nm, 1.5 W cm^{-2}), followed by switching off the laser; Linear fitting between the cooling time data versus -ln(θ) (the negative natural logarithm of the temperature driving force) of DTPA-TBZ dots (B) and DTPA-BBTD dots (C), which was calculated from the system cooling period in (A).

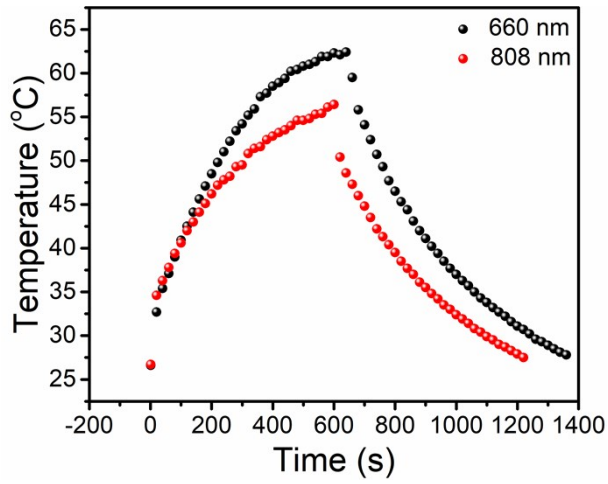

Figure S12. Photothermal heating and cooling curves of DTPA-BBTD-based AIE dots ([*c*]= 200 μg/mL) upon 660 nm and 808 nm laser irradiation, respectively, followed by switching off the laser.

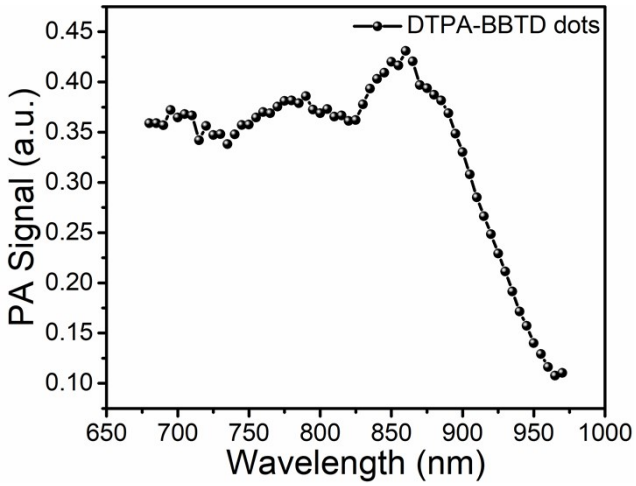

Figure S13. PA signals for DTPA-BBTD-based AIE dots in centrifugal tube under different wavelength.

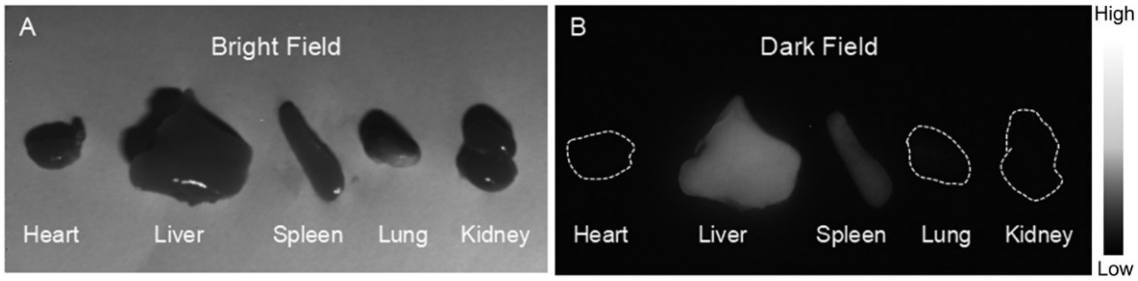

Figure S14. The bright field image (A) and fluorescence image obtained by the NIR-II imaging system (B) for major organs in BALB/c nude mice.

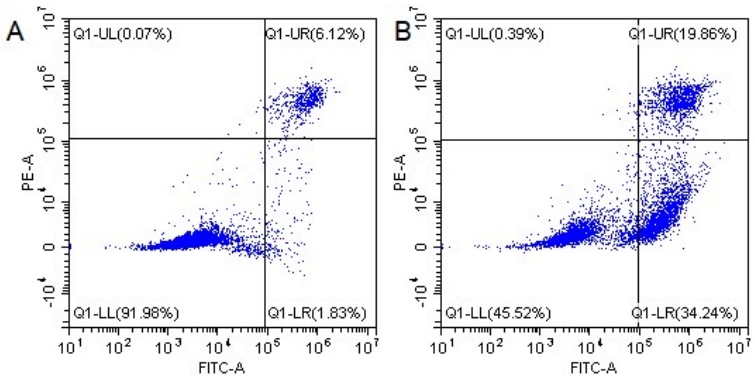

Figure S15. Apoptosis and necrosis of Hela cells analyzed by flow cytometry to determine the percentages of apoptosis and necrosis; HeLa cells were incubated with PBS (A: control) and DTPA-BBTD dots + Laser (30 μg mL^{-1}) for 24 h (Q1-UL: necrotic cells; Q1-UR: late apoptotic cells; Q1-LR: early apoptotic cells; Q1-LL: living cells).

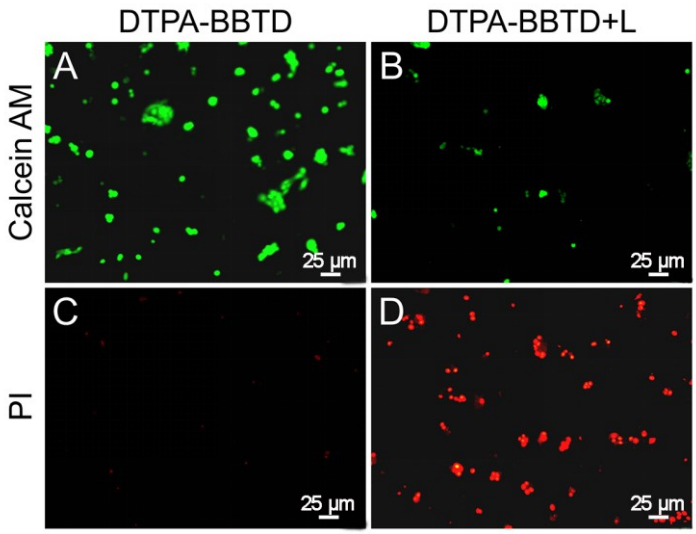

Figure S16. Live/dead assays of 4T1 cells treated with DTPA-BBTD-based AIE dots without (A: live assay; C: dead assay) or with irradiation (B: live assay; D: dead assay).

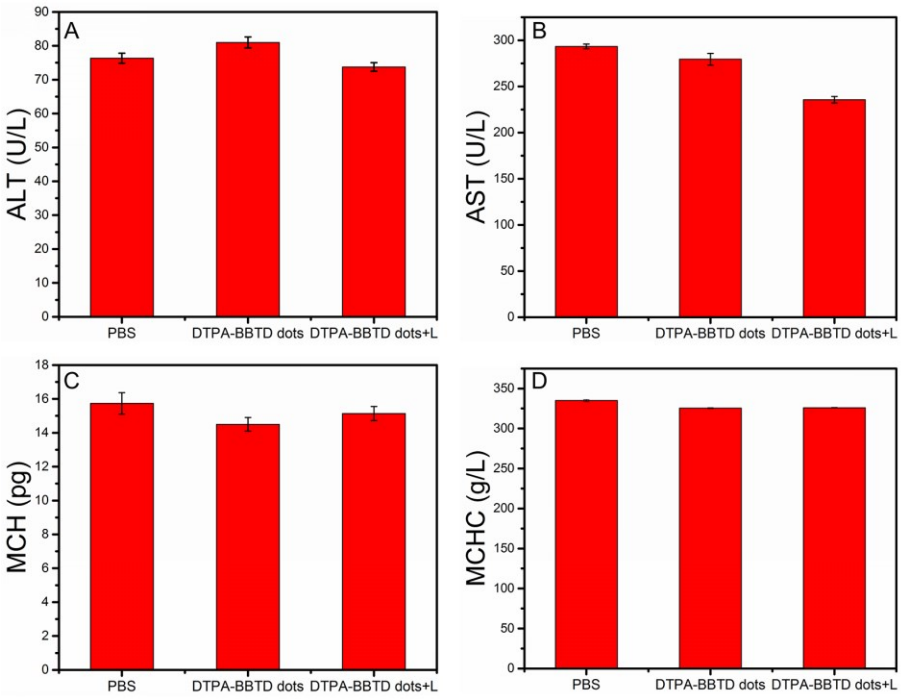

Figure S17. Hematological parameters, including aminotransferase (A, ALT), aminotransferase (B, AST), mean corpuscular hemoglobin (C, MCH), mean corpuscular hemoglobin concentration (D, MCHC) for BALB/c nude mice injected by PBS solution and DTPA-BBTD-based AIE dots with/without laser.

NMR and Mass spectra

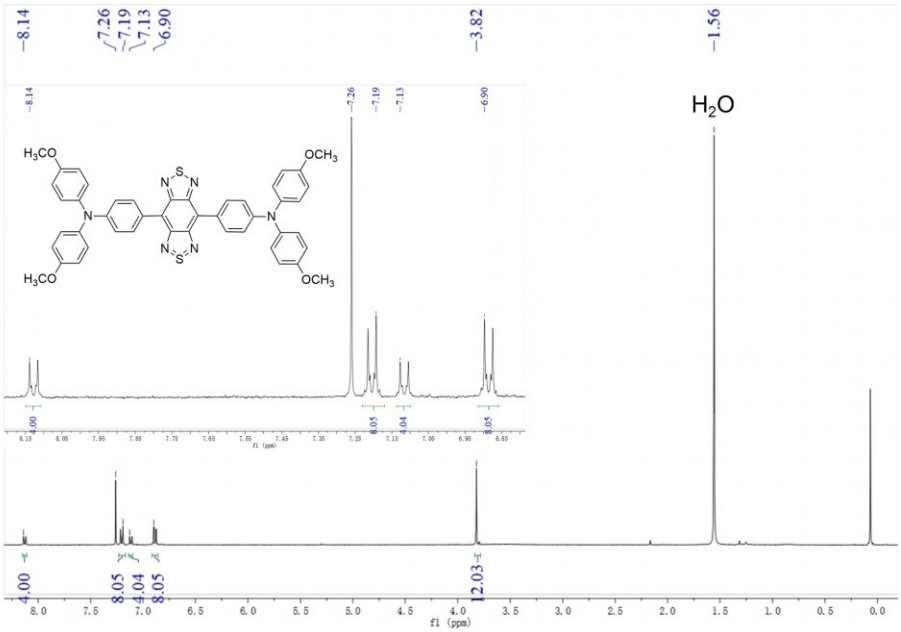

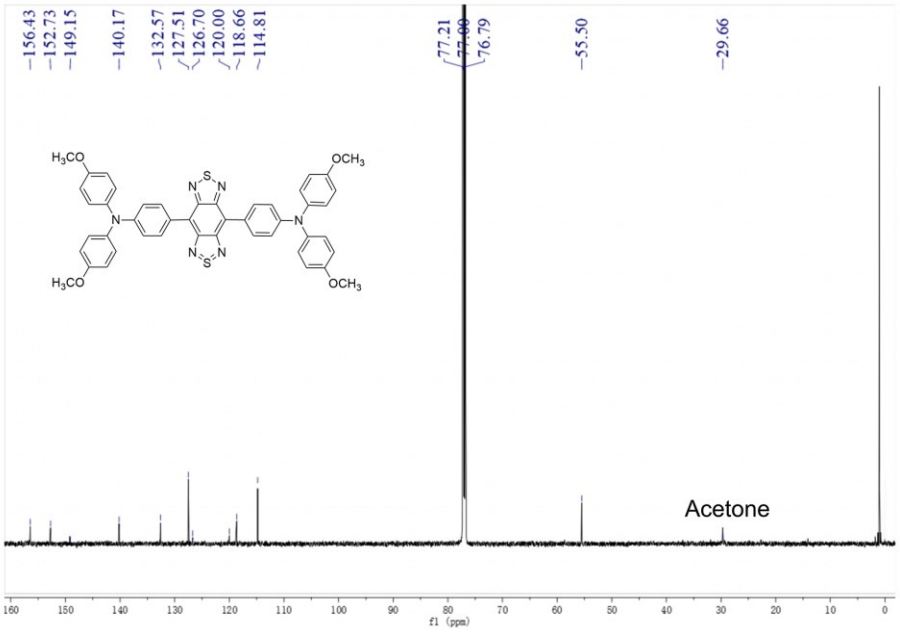

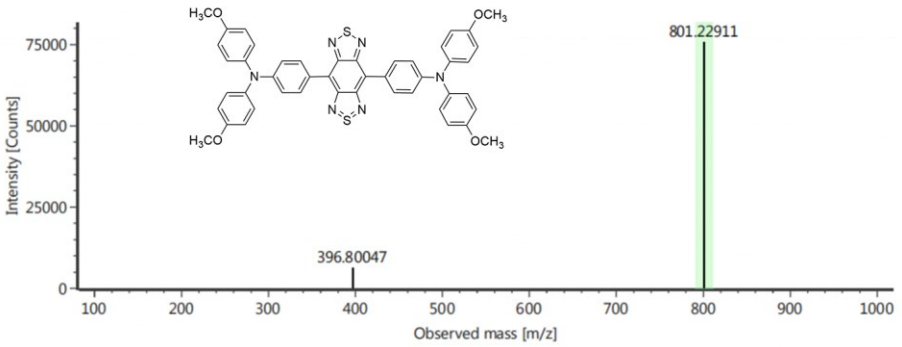
801.22911
396.80047
Intensity [Counts]
Observed mass [m/z]

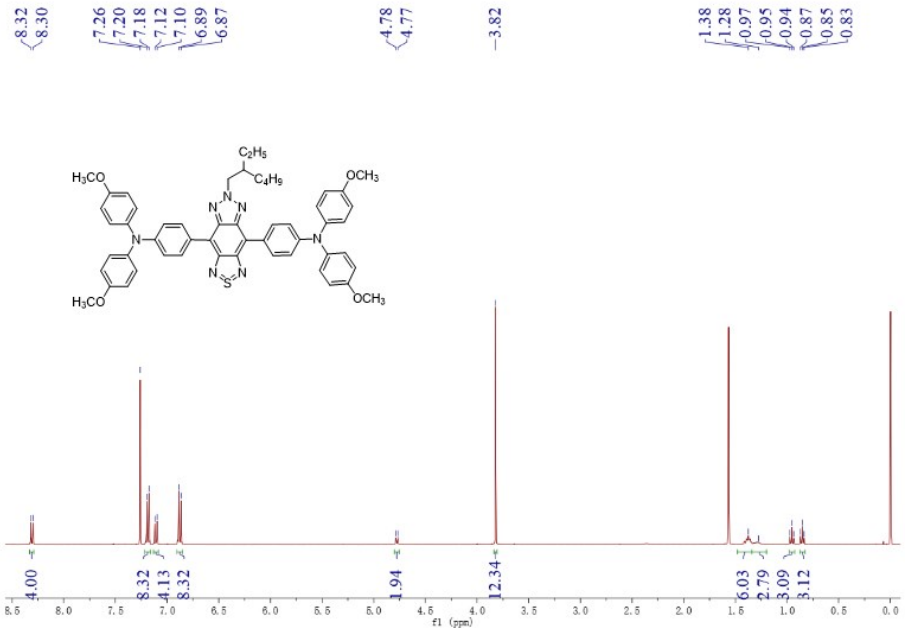
8.32
8.30
7.26
7.20
7.18
7.12
7.10
6.89
6.87
4.78
4.77
3.82
1.38
1.28
0.97
0.95
0.94
0.87
0.85
0.83
4.00
8.32
4.13
8.32
1.94
12.34
6.03
2.79
3.09
3.12
f1 (ppm)

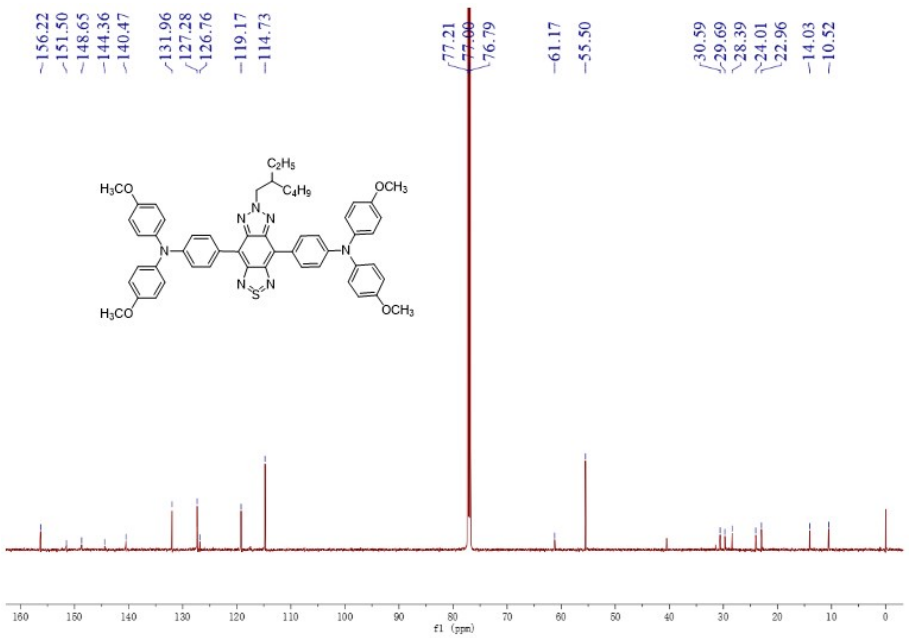
156.22
151.50
148.65
144.36
140.47
131.96
127.28
126.76
119.17
114.73
77.21
77.00
76.79
61.17
55.50
30.59
29.69
28.39
24.01
22.96
14.03
10.52
f1 (ppm)

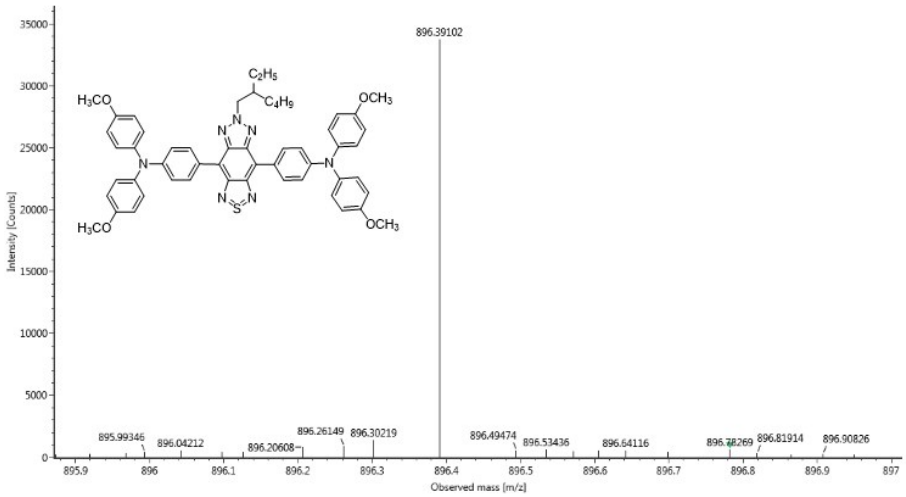

Reference

[1] Yanzi Xu, Chunbin Li, Ruohan Xu, Ning Zhang, Zhi Wang, Xunan Jing, Zhiwei Yang, Dongfeng Dang, Pengfei Zhang, Lingjie Meng, *Chem. Sci.*, 2020, **11**, 8157.

[2] Dong Wang, Michelle M. S. Lee, Wenhan Xu, Guogang Shan, Xiaoyan Zheng, Ryan T. K. Kwok, Jacky W. Y. Lam, Xianglong Hu, Ben Zhong Tang, *Angew Chem. Int. Ed.*, 2019, **58**, 5628.

[3] Dongfeng Dang, Xiaochi Wang, Daquan Wang, Zhiwei Yang, Dongxiao Hao, Yanzi Xu, Shengli Zhang, and Lingjie Meng, *ACS Appl. Nano Mater.,* 2018, **1**, 2324.